Soils and Rocks
An International Journal of Geotechnical and Geoenvironmental Engineering
www.soilsandrocks.com
ISSN 1980-9743
ISSN-e 2675-5475

Internal erosion initiation processes in homogeneous earth fill dams: a case study

Conrado Oliveira Carestiato de Carvalho[1#], Tácio Mauro Pereira de Campos[1], Álvaro de Freitas Viana[2]

Case Study

Keywords
Earth fill dam
2D water flow
3D water flow
Unsaturated flow
Internal erosion

Abstract

In a homogeneous earth fill dam, an initial process of internal erosion was observed near the base of the downstream slope, which is one of the main dam failure causes in the world. This problem was adequately solved, and research was started aiming to find the causes of the detected anomaly. The history of the structure was investigated, field testing results were analyzed and undisturbed samples were collected in different regions of the dam. Characterization tests, saturated permeability coefficients tests under different effective stresses and flow directions, and Filter Papel tests were run. Results were incorporated into computational models to investigate the behavior of hydraulic gradients and the height of the exit point of the phreatic line defined on the basis of monitored piezometers installed at the site. The software Plaxis LE was used in this study. It was evaluated whether the adoption of unsaturated parameters or 3D analysis would promote any change in the flow pattern in the studied structure, which did not occur. It was also considered whether the soil-atmosphere interaction could generate critical hydraulic gradients through rainfall and evaporation cycles, but there were no critical results either. Finally, it is concluded that effects of natural vegetation previously found in Dam X may have led to the observed internal erosion process. These somewhat unusual findings are relevant for improving the understanding of vegetation impacts on earth dam safety and can help guide future monitoring and, particularly, maintenance practices to prevent similar issues in other similar earth fill dams.

1. Introduction

Internal erosion has been considered one of the most common dam failure modes. Considering exclusively water-retained structures, Foster et al. (2000) mention that 46.1% of dam failures until 1986 were caused by internal erosion processes. This failure mode occurs when flux lines concentrate near a small region, leading to an increase in hydraulic gradients, *i* (Foster & Fell, 1999; Fell et al., 2003; Taher & Alshibli, 2015). Considering embankments built to retain non-inert solids or liquids, eventual failures due to internal erosion are also to be expected. In these cases, however, processes are not necessarily related to increased hydraulic gradients, but to the chemical characteristics of the flowing fluid (e.g. high or low pH) through poorly protected, or even unprotected, upstream slope of the embankment (e.g. Mungan, 1965; Suarez et al., 1984; Moncada et al., 2005; Carvalho et al. 2006; Xu et al., 2020).

Considering exclusively water-retained structures, several authors discuss which soil properties may contribute to the generation of an internal erosion process (piping processes). Perry (1975) evaluated that until late 1950s, engineers believed that resistance to erosion was associated with soils' intrinsic parameters and constructive methods. Sherard (1953) studied the influence of the plasticity index and evaluated that resistance to internal erosion increases when plasticity increases. De Mello (1975) and Foster & Fell (1999) pointed out that internal instability is more susceptible to occur in gap-graded soils or well-graded soils with smooth gradation but a flat tail in the fine portion (silty and clay). It is also well known that dispersive clays are prone to piping development (Sherard et al., 1976; Turgut et al., 2017).

Practical methods based on filter criteria as first proposed by Terzaghi (Terzaghi et al., 1996) to evaluate soil internal instability, and its potential to develop an internal erosion process have been put forward by several authors (e.g. Kezdi,

[#]Corresponding author. E-mail address: conrado_cocc@hotmail.com
[1]Pontifícia Universidade Católica do Rio de Janeiro, Departamento de Engenharia Civil e Ambiental, Rio de Janeiro, RJ, Brasil
[2]ALTA Geotecnia Ambiental, Rio de Janeiro, RJ, Brasil

Submitted on November 3, 2023; Final Acceptance on January 6, 2025; Discussion open until May 31, 2025.
Editor: Renato P. Cunha
https://doi.org/10.28927/SR.2025.010923

1979; Sherard, 1979; Vaughan & Soares, 1982; Kenney & Lau, 1985; Li & Fannin, 2008; Delgado-Ramos et al. 2012).

This article investigates the possible causes of an initial internal erosion process found in an earth fill dam, whose reservoir is used for water supply in a Brazilian industrial site. During a visual inspection, a region on the downstream face of the dam, located at approximately 1/3 of the dam height (from its toe), was observed to be saturated. Furthermore, it was verified occurrence of fine particles being carried away by seepage in the drainage system installed at the downstream slope toe of the dam.

2. Materials and methods

2.1 Study dam

The main structure herein considered, named Dam X, comprises a 9 m high, some fifty years old, homogeneous earth dam. Its crest is 5m wide. It supports an operational water volume of approximately 160.000 m^{3,} and it has an "L" format in the horizontal plane (Figure 1) with some 175 m in its front (South) and some 155 m in its lateral part (East). Downstream slope inclination is 1(V):2(H), while upstream slope is 1(V):3(H).

No detailed or even basic design documentation for Dam X was identified. Only some photos taken between December 1970 and June 1972, when construction took place, were made available by the owners of the site (see Figure 2). Based on these photos and information provided by old employees from the industry, it was possible to identify that a cutoff excavation, with internal slopes of 45°, estimated to be 10 m large and 3 m depth, was introduced at the south end of the embankment.

Dam X was constructed within a rainforest environment, in a valley surrounded by mountain cliffs. As the structure was built over an original course of a stream, an outlet pipe was built bellow the south embankment, and a side channel uncontrolled spillway was introduced upstream of the formed reservoir (see Figure 1).

In 2015, Dam X's downstream slopes were covered by vegetation by the lack of proper maintenance procedures for the structure (Figure 3). As discussed later, such an aspect may have a relevant role in the already mentioned observation of fine particles being carried away in the drainage system installed at the downstream slope toe of the dam (Figure 4).

Although not discussed in the present work, it is relevant to mention that the observed problem was solved in 2020 by introducing an inverted filter and a drainage system at the downstream slope toe.

2.2 Investigations and monitoring data

Field investigations comprised SPT and hand auger boreholes, execution of trenches with block sampling, and

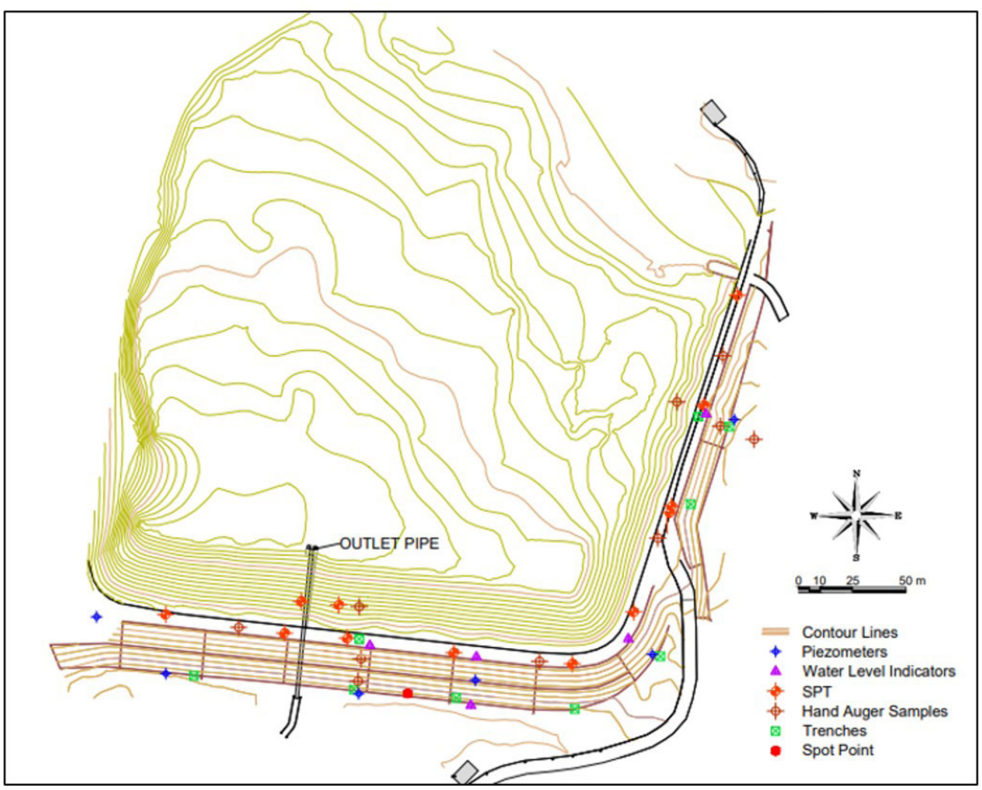

Figure 1. Plane view of Dam X.

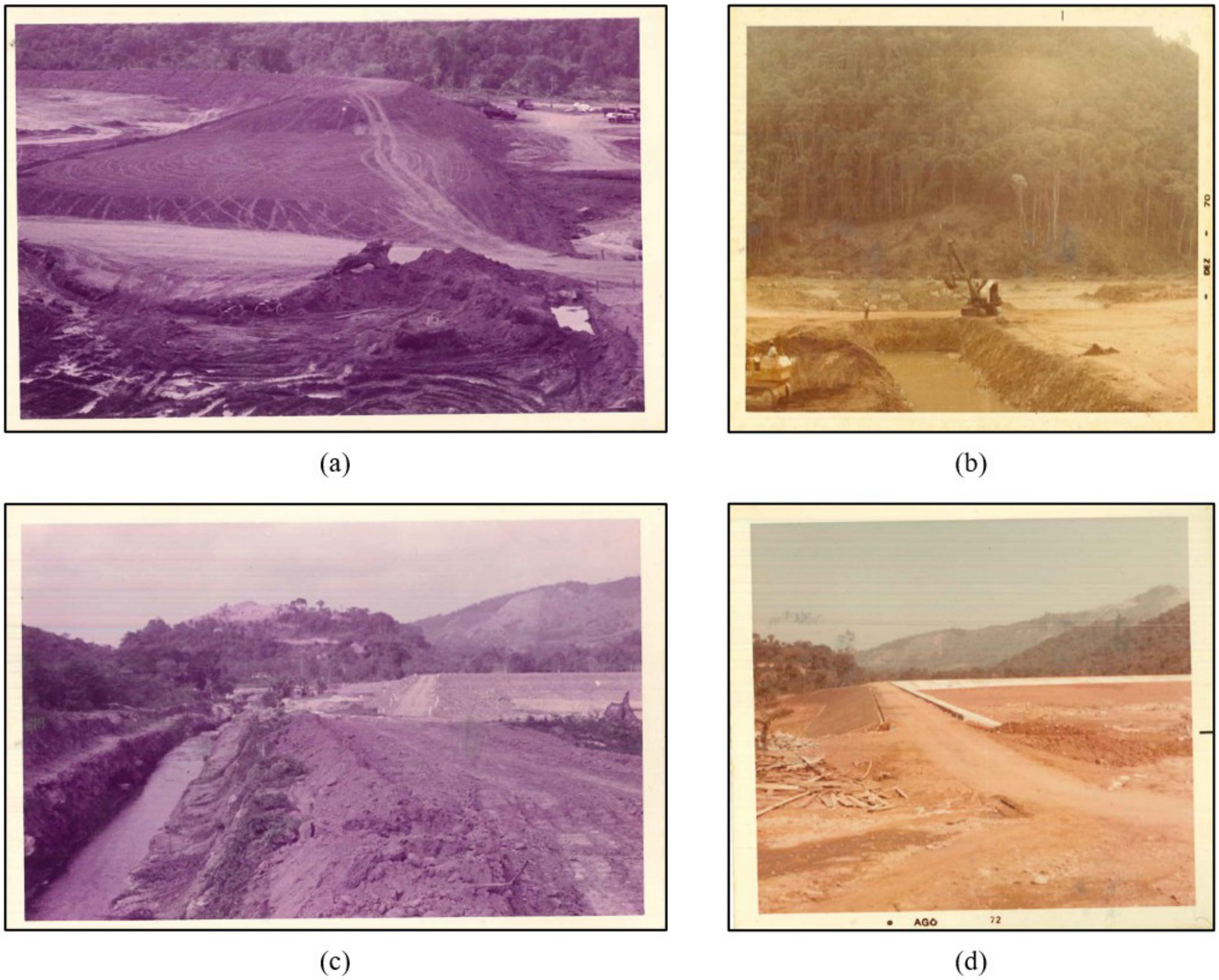

Figure 2. (a) Dam X construction, using only soil available at the site; (b) and (c) Cutoff excavation; (d) Dam X upstream view in August 1972.

installation of instrumentation at the points shown in Figure 1. These investigations indicated a relatively homogeneous section for Dam X. The Dam foundation comprises a granite-gneissic residual soil, described as a medium to fine silty sand.

Undisturbed block samples were collected at different depths of the embankment and near the point where seepage was carrying fine particles (spot point - refer to Figure 1). Laboratory investigations comprised conventional characterization tests following Brazilian Standards (ABNT, 2016a, b, c, 2017, 2018), which are similar to corresponding US standards; saturated, constant head flexible wall permeability tests (based on Head, 1994) and soil moisture retention or soil-water characteristic curve using the filter paper technique (ASTM, 2016).

2.2.1 Soil characterization

Table 1 shows the results of characterization tests performed on the material retrieved near the spot point. These results are, on average, representative of those of the other

Figure 3. Dam X's downstream slope covered by vegetation, in 2015.

Table 1. Spot point soil characterization.

G_s	Gravel (%)	Sand (%)			Silt (%)	Clay (%)	w_L (%)	w_P (%)	*PL* (%)	A_c
		Coarse	Medium	Fine						
2.66	2.6	1.1	37.2	15.5	25.3	18.3	44.6	28.2	16.5	0.9

Figure 4. Evidence of fine particles being carried away in the drainage system installed at the downstream slope toe of the dam (photo taken in 2018).

points of investigation (De Carvalho, 2022). Such material is classified in the USCS as a clayey sand (SC), with fines showing a normal activity A_c. Considering its grain size distribution (Figure 5), it does not represent a gap-graded soil. Furthermore, results of chemical analysis developed at PUC-Rio on materials similar to that herein considered (e.g. Oliveira, 2006), have shown that bivalent cations are essentially associated with their finer fraction, which indicates that it is little or no susceptible to dispersivity (Keaton, 2018). So, in principle, it can be considered that this soil is not susceptible to natural internal erosion processes.

Table 2 shows average physical indexes of undisturbed tested samples retrieved at different depths and near the spot point of Dam X. It can be seen that physical indexes at the spot point are similar to those obtained from different parts of the Dam. However, while the landfill, as a whole, is unsaturated (S = 78.6%) the spot point is close to saturation. Thus, considering the spot point, the critical hydraulic gradient (i_{cr}), defined as the ratio between the specific weights of the water and of the submerged soil has been computed as 0.93.

2.2.2 Permeability

Horizontally and vertically molded specimens were used to determine the saturated permeability of the block samples taken from different depths of the dam (Table 3). At the spot point, the saturated permeability coefficient was determined from specimens molded under three orthogonal directions: horizontal, aligned with the dam axis (Longitudinal) and transverse to dam axis (Transversal), and vertical. For each direction, tests were run under three different effective stresses: 10, 50 and 100 kPa, and their average was obtained (Table 4).

2.2.3 Soil-water retention curve

Figure 6 shows the soil-water retention curve (SWRC) obtained, which presents a unimodal pattern. The fitting curve adjusted to the laboratory data was based on Fredlund & Xing (1994).

2.3 Seepage analyses

2D and 3D seepage analyses, considering unsaturated materials and permanent and transient regimes, were performed using the software Groundwater of Plaxis LE from Bentley Systems. In the 2D analyses, a cross-section of Dam X was modeled considering an upstream slope with an inclination of 1(V):3(H) and the downstream slope with an inclination of 1(V):2(H). Foundation soil was modeled with a thickness of 4 m. In 3D analyses, a digital terrain model was created with Plaxis Design software based on previous topographic studies of the region, see De Carvalho (2022) for details.

Including the third dimension in seepage analyses demands a permeability value for each direction. The software requires the X-axis permeability (in this paper considered to be horizontal and longitudinal to the dam axis), and two anisotropy factors: one for the Y axis (also horizontal but transversal to the dam axis) and another to the Z axis (vertical). The adopted values are shown in Table 5.

The climatic data for the transient unsaturated analyses, which are temperature, relative humidity, wind speed, solar radiation and pluviometry, were collected from an INMET (Brazil's National Institute of Meteorology,) automatic station, 4 km away from Dam X (see De Carvalho 2022 for details). Furthermore, unsaturated water conductivity functions were defined based on Fredlund & Xing (1994) using facilities included in the software Plaxis LE.

Finite element meshes discretization were evaluated, being considered the ones in which no more changes in the phreatic line occurred. Figure 7 shows adopted boundary conditions used in the 2D and 3D analyses. Flow through the foundation was not considered. Thus, upstream and downstream limits of adopted impermeable boundaries were defined when they did not affect anymore seepage results within the Dam.

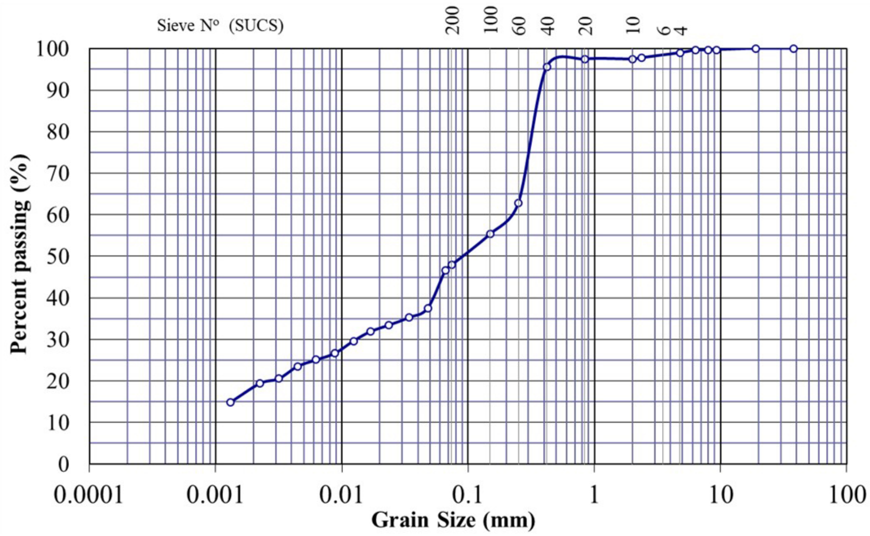

Figure 5. Grain size distribution curve of the soil at the spot point.

Table 2. Average in situ physical indexes at different depths and at the spot point.

Sample	G_s	w (%)	γ_t (kN/m³)	γ_d (kN/m³)	e	S (%)
Variable depth	2.58	19.7	18.79	15.70	0.68	78.6
Spot point	2.66	26.1	18.91	15.00	0.74	93.4

Table 3. Permeability of samples taken from different depths of the Dam.

Sample Depth (m)	k_{sat} (10^{-8} m/s)	
	Vertical	Horizontal
1.5	25.7	20.3
2.5	14.6	1.91
4.2	8.29	3.96
5.0	27.9	1.24
Average	19.1	6.85

Table 4. Average permeability test results at the spot point.

k_{sat} (10^{-8} m/s)		Effective Stress (kPa)		
		10	50	100
Horiz.	Transversal	9.72	2.17	1.17
	Longitudinal	4.03	0.42	0.18
Vertical		1.20	0.45	0.29

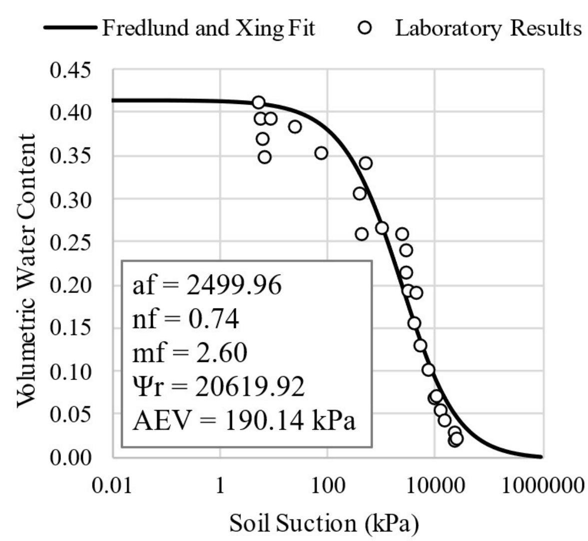

Figure 6. SWRC laboratory data with Fredlund & Xing (1994) fitting curve and adjusting parameters.

2.4 Dam instrumentation

Dam X was instrumented with Casagrande piezometers (PZC) and water level indicators (WL) (Figure 1). The pore water pressure distribution in a section of the dam crossing such a point was based on data from instruments located near the spot point (Figure 8). The phreatic line reaches the downstream slope of the Dam at a height of circa 3.0 m above the toe of the downstream slope (Figure 8).

Table 5. Saturated permeability values adopted for 3D seepage analyses.

Materials	Longitudinal permeability (X-axis) (m/s)	Transverse permeability (Y-axis) (m/s)	Vertical permeability (Z-axis) (m/s)	Transverse anisotropy factor	Vertical anisotropy factor	Scenarios of use
Varying with depth average	6.85×10^{-8}	6.85×10^{-8}	1.91×10^{-7}	1.00	2.79	1
σ' = 10 kPa	4.00×10^{-8}	9.72×10^{-8}	1.20×10^{-8}	2.41	0.30	2 and 3
σ' = 50 kPa	4.20×10^{-9}	2.20×10^{-8}	4.50×10^{-9}	5.14	1.05	2
σ' = 100 kPa	1.80×10^{-9}	1.20×10^{-8}	2.90×10^{-9}	6.32	1.57	2 and 4
Average Parameters	1.50×10^{-8}	4.35×10^{-8}	6.45×10^{-9}	2.81	0.42	2
Foundation	3.69×10^{-8}	3.69×10^{-8}	3.69×10^{-8}	1.00	1.00	All

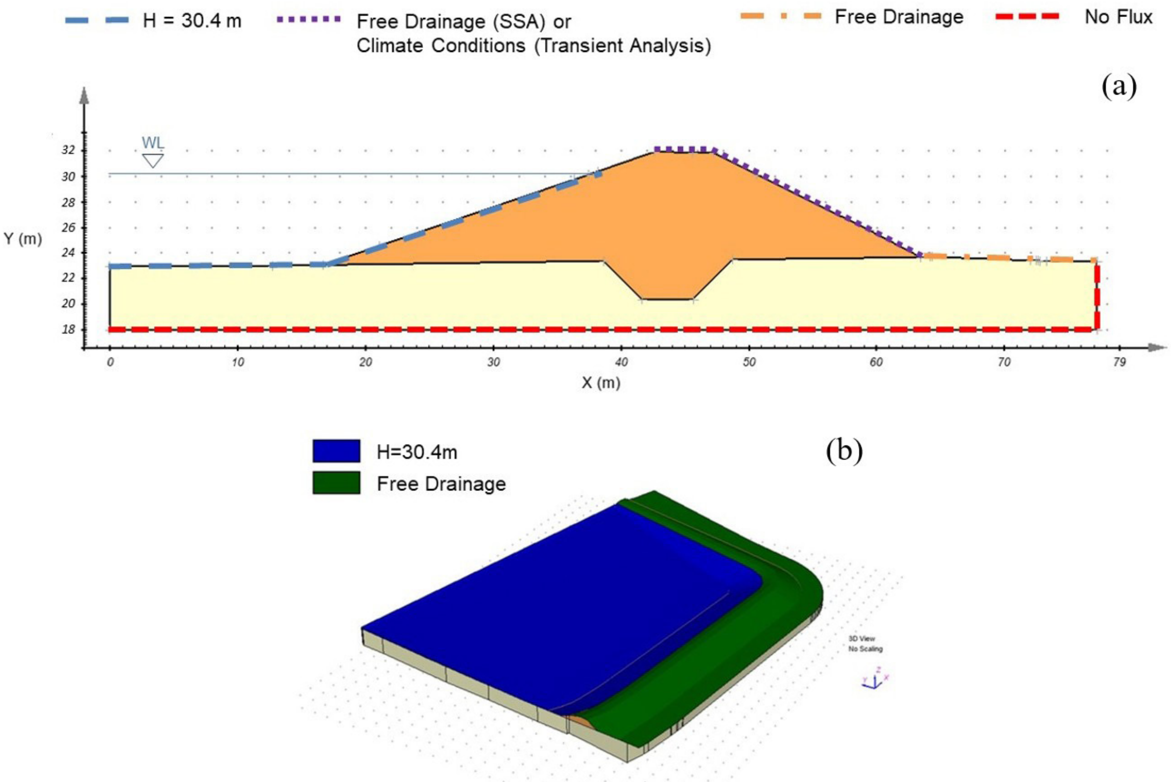

Figure 7. Adopted boundary conditions (a) 2D analyses, (b) 3D analyses.

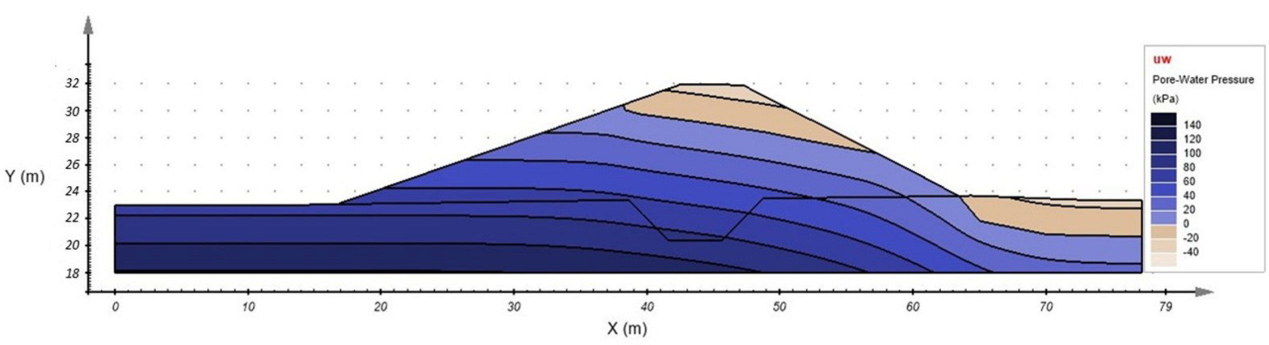

Figure 8. Pore-water pressure distribution in a section crossing the spot point, defined based on the site instrumentation, assuming a saturated dam condition.

2.5 2D analysis

To investigate the distribution of hydraulic gradient through Dam X's cross-section, three 2D seepage conditions were analyzed: saturated steady-state flux, unsaturated steady-state flux and steady-state and transient unsaturated flux. As no differences were obtained in the steady-state saturated and unsaturated flow analyses, only results under unsaturated conditions are here presented.

Considering a steady-state unsaturated flux condition, four different 2D scenarios were evaluated:

- Scenario 1: Analysis considering permeability parameters from different depths (Table 3);
- Scenario 2: Discrete permeability variation from dam surface, adopting k_{sat} at $\sigma' = 10$, 50 and 100 kPa (Table 4);
- Scenario 3: Homogeneous earth fill dam considering k_{sat} at $\sigma' = 10$ kPa;
- Scenario 4: Homogeneous earth fill dam considering k_{sat} at $\sigma' = 100$ kPa.

Also, a transient analysis was implemented to evaluate whether the soil-atmosphere interaction on the downstream slope could change Dam X's seepage pattern. Two different periods were analyzed: January and September of 2018. The first was selected because it is historically the month with the highest pluviometry index for the region. The second one was chosen because it was when the carrying of fines process was identified. It also represents the lowest rainy season at the site.

2.6 3D analysis

Scenarios 2 to 4 for 2D analysis were also considered in a 3D configuration. Additionally, two new scenarios were considered. The first (Scenario 5) aimed to evaluate the possibility of having a material near the downstream slope toe with a hydraulic conductivity that could lead to the occurrence of critical gradients. For that, it was assumed the occurrence of a material with a different permeability coefficient at a region corresponding to one-third of the maximum height of the dam, above the toe of the downstream slope. The second (Scenario 6) simulated the occurrence of a 1 to 4 m wide section, also with variable permeability conditions, crossing the spot point of Dam X. As no relevant differences were found, only results related to a 1 m wide section are here presented.

Saturated permeability values in both scenarios were varied as: (i) hydraulic isotropic material, (ii) horizontal permeability fixed (as Table 3 average value) and vertical varied, (iii) vertical permeability fixed (as Table 3 average value) and horizontal varied.

3. Results and discussion

3.1 2D steady-state analyses results

Table 6 shows the height of the phreatic line exit point (PLEP) and values of hydraulic gradient resulting from the steady-state seepage analyses. The height of the PLEP varies directly with the transversal permeability. The highest value was found in Scenario 3, in which $k_h = 9.70\text{x}10^{-8}$ m/s. However, the same trend is not observed for the hydraulic gradient. Considering only scenarios 3 and 4, with homogeneous cross-sections, this parameter increases while the permeability coefficient decreases.

Critical hydraulic gradients (values above 0.93) were found at the dam slope surface. However, as put forwards by Babu & Vasudevan (2008) and Bernatek-Jakiel et al. (2017), such values may not be considered as representative due to the presence of vegetation on the dam surface. So, hydraulic gradients found at 15 cm deep from the dam slope surface is hereby considered to be more representative for Dam X. In that case, as indicated in Table 6, hydraulic gradients were not critical and varied little, being higher for Scenario 3.

Referring to Table 5, even though Scenarios 1 and 4 have similar horizontal permeability parameters, the height of PLEP and the hydraulic gradient distribution are different. This can be explained by differences between vertical permeabilities: on Scenario 1, the vertical permeability is 66 times higher than on Scenario 4. This shows the relevance of considering aspects of permeability anisotropy in seepage analyses. Considering the available Dam X instrumentation data, Scenario 3 was the most representative concerning the exit point of the phreatic surface (Figure 8).

It is of interest to point out that the results of 2D analyses indicated that FEM mesh size influences hydraulic gradient values without any relevant effects on the position of the PLEP. As indicated in Figure 9, as the mesh element area is reduced, the maximum hydraulic gradient value increases. At the same time, the height from the downstream slope at which such maximum gradients occur increases with increasing mesh element areas.

Such a feature was observed by running tests using two different software packs that employ FEM to solve numerical analyses: Plaxis LE, from Bentley Systems, and Slide2, from Rocscience. By considering flow nets, the definition of hydraulic

Table 6. 2D steady-state unsaturated seepage analyses results.

Scenario		1	2	3	4
Height of phreatic line exit point (*PLEP*) (m)		1.75	1.84	3.26	0.98
Downstream slope hydraulic gradient	Maximum value at the slope surface	0.61	1.00	1.26	1.60
	10 cm above toe (superficial)	0.59	0.60	0.78	0.86
	15 cm deep from slope surface	0.55	0.46	0.57	0.56

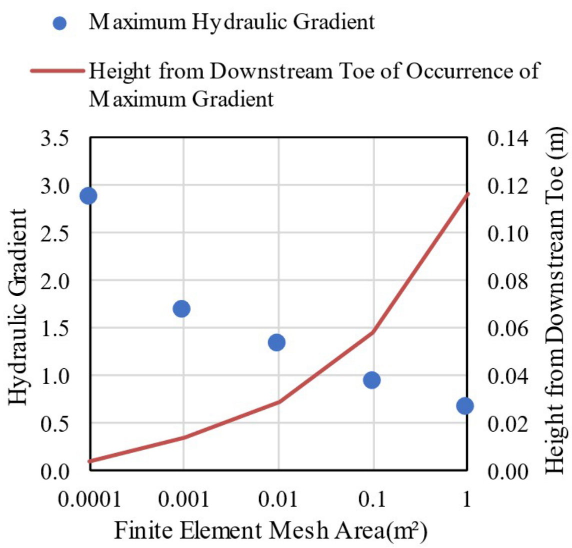

Figure 9. Maximum hydraulic gradient variation on downstream slope surface *versus* FEM mesh discretization.

gradients based on finite element areas may be seen with care, as such gradients are defined based on the distance between two consecutive equipotential lines along a given flow line.

3.2 2D transient analyses results

As Scenario 3 was more credible to the situation indicated by Dam X instrumentation, it was considered for the transient analyses. The adopted initial pore water pressure distribution is shown in Figure 8. Figure 10 shows the hydraulic gradient variation at a point 15 cm deep of the downstream slope, near its toe, with precipitation data for the months considered.

Throughout January 2018, the difference between maximum and minimum gradient is around 0.04. This parameter tends to increase when pluviometry increases. The effect of rain on the analyzed parameter seems to be lagged, but Figure 10 shows that gradients increase after rain occur and decreases when there is lower or no precipitation.

In September 2018 there was a larger reduction of the hydraulic gradient compared to results from January, with a minimum gradient of 0.645 around the 13th day of the month. After four subsequent rainy days, *i* rises until values close to the initial condition, reaching its peak at 0.682.

Comparing the results of the steady state and the transient 2D analysis for the climatic conditions considered, rainwater infiltration at the downstream slope of Dam X did not promote any relevant change in the flow pattern.

3.3 3D steady-state analyses results

Table 7 shows the hydraulic gradient distribution near the downstream slope toe of Dam X and the height of the PLEP obtained in the 3D analyses near the Spot Point.

Comparing Tables 6 and 7, the height of the PLEP is similar. However, the 3D approach generated, in general, around 4% lower heights.

Regarding the hydraulic gradient, maximum values found in 3D analyses were higher than in the 2D analyses. Considering an elevation 10 cm above Dam X toe, 3D results were some 5% higher. At a depth of 15 cm below the downstream slope, 3D results are some 3% higher. Even though, critical hydraulic gradients were not observed. Thus, 3D additional analyses were developed.

Figures 11 and 12 show how the height of the PLEP and the hydraulic gradient varied with the assumed changes in the saturated hydraulic conductivity for, respectively, scenarios 5 and 6.

It can be seen in Figure 11a that the hydraulic gradient on the downstream slope surface increases from 0.61, for k_{sat} = 9.7x10^{-8} m/s, to 2.22, for k_{sat} = 4.0x10^{-11} m/s. Considering a section crossing the spot point (Figure 12a), the gradient fluctuates between 0.59 and 1.54. In both scenarios, at a point 15 cm deep, the hydraulic gradient behaves similarly to the surface but with lower values. Critical gradients occur for isotropic permeabilities lower than 1.2x10^{-8} m/s in Scenario 4 and 1.0x10^{-9} m/s in Scenario 5.

In Scenario 5, when critical gradients are generated in-depth, the height of the PLEP varies less than 10 cm up to hydraulic coefficients of the order of 10^{-8} m/s. With increased k_{sat}, the PLEP height decreases exponentially (Figure 11a). In Scenario 6, the height of the PLEP did not show any relevant change (Figure 12a).

In Figures 11b, 11c, 12b and 12c, saturated permeability values shown in Table 3 were used as reference. In Figures 11b and 12b horizontal coefficient was fixed on 6.85x10^{-8} m/s and vertical permeability increased and decreased by 1000 times, in steps of 10. In Figures 11c and 12c the vertical coefficient was fixed on 1.91x10^{-7} m/s and horizontal permeability was varied from 1.91x10^{-4} to 1.91x10^{-10} m/s.

Figures 11b and 12b show pattern of curves similar to those of Figures 11a and 12a. In Scenario 5 (Figure 11b) for permeability coefficients higher than 1.0x10^{-}7 m/s, hydraulic gradients were kept around 0.5, both on the surface and in-depth. If vertical permeability decreases, the gradient gets higher and reaches 1.34, on the surface, and 0.81, in depth, for permeability lower than 1.0x10^{-9} m/s. A similar response is obtained in Scenario 6 (Figure 12b), with slightly lower hydraulic gradients being obtained both on the surface and at 15 cm depth.

The height of PLEP increases when the vertical permeability decreases, reaching its peak at 2.56 m for permeability coefficients lower than 1.0x10^{-9} m/s in Scenario 5 (Figure 11b) and at a higher height (1.5 m) in Scenario 6 (Figure 12b), for a permeability coefficient of 6.85x10^{-11} m/s.

Figure 11(c) indicates that the phreatic line reached the downstream slope surface at a height less than 0.5 m above its toe, for a permeability ratio lower than 0.1 (representing horizontal permeabilities higher than 1.0x10^{-5} m/s). The height

Table 7. 3D steady-state unsaturated seepage analyses results.

Scenarios		2	3	4
Height of PLEP (m)		1.82	3.06	0.92
Downstream slope hydraulic gradient	10 cm above toe (superficial)	0.63	0.80	0.90
	15 cm deep from slope surface	0.48	0.58	0.59

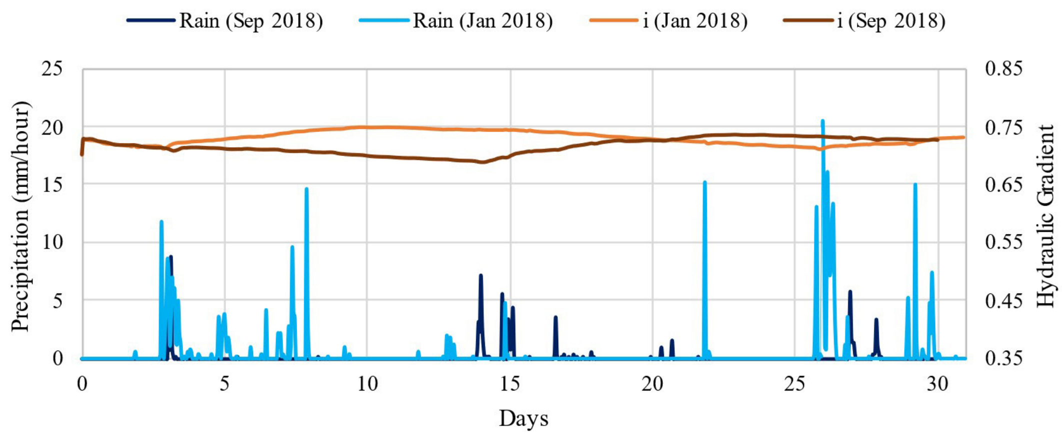

Figure 10. Hydraulic gradient variation throughout January and September of 2018 at a point 15 cm deep from the downstream slope of Dam X, near its toe.

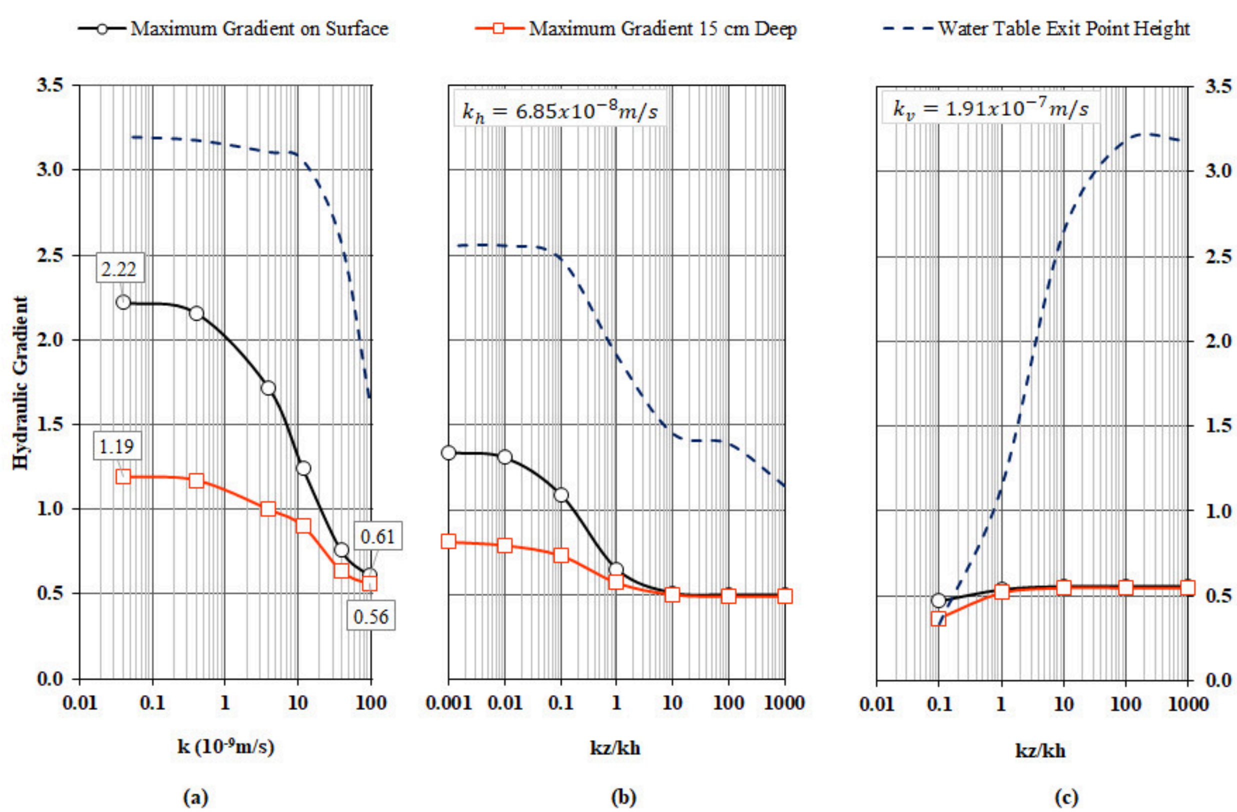

Figure 11. Scenario 5: (a) Isotropic permeability variation influence, (b) Vertical permeability variation influence, (c) Horizontal permeability variation influence.

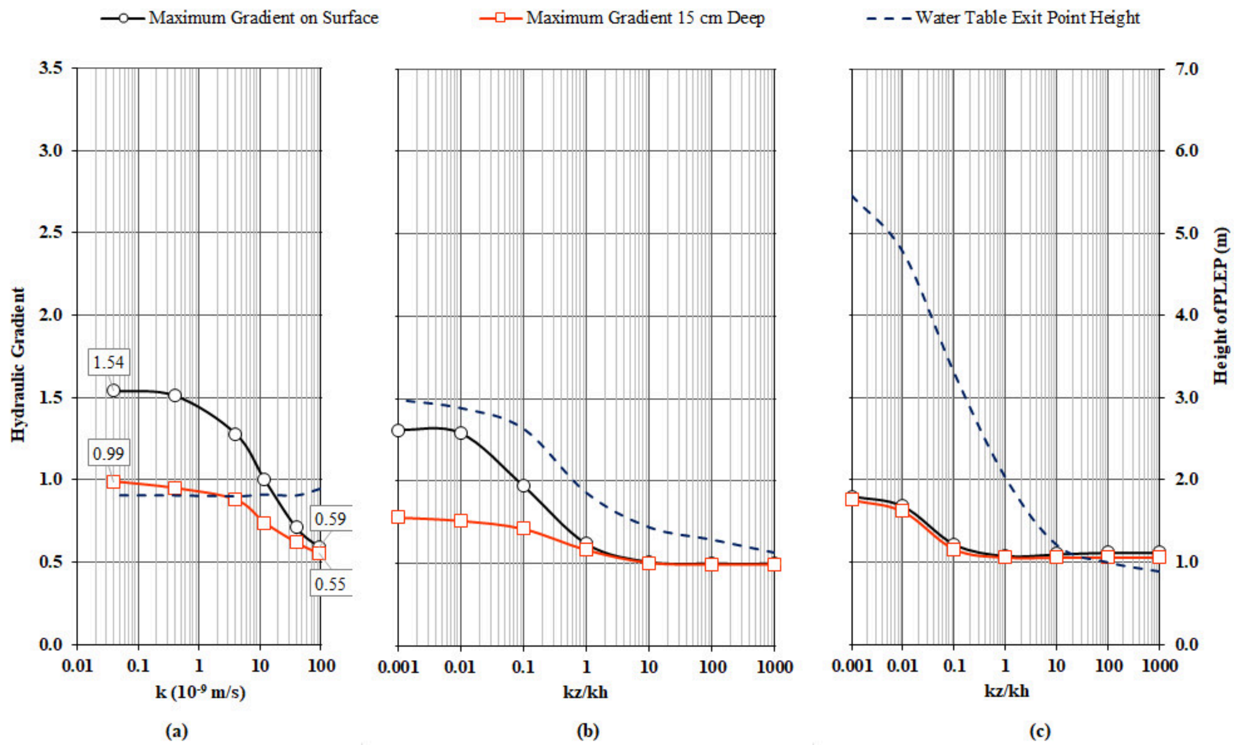

Figure 12. Scenario 6: (a) Isotropic permeability variation influence, (b) Vertical permeability variation influence, (c) Horizontal permeability variation influence.

of the PLEP rises for higher anisotropy ratios, reaching 3.18 m for horizontal permeability lower than 1.0x10^{-9} m/s (ratio greater than 1.000 in Scenario 5). Hydraulic gradients kept approximately the same value, both on the surface and in-depth, around 0.55. On the other hand, variations in k_{hor} in Scenario 6 indicated that the height of the PLEP reaches higher values when horizontal permeability increases (Figure 12c). Also, hydraulic gradients get lower when horizontal permeability decreases (and the anisotropic ratio increases).

3.4 Discussions

This work presents results of flow analyses in the Dam X embankment, which shows an average degree of saturation of 79%. Owing to this relatively high degree of saturation and the relatively high air entry suction value of the Dam material (order of 100 kPa, see Figures 6) it is not surprising to have been verified that 2D analyses assuming the Dam fully saturated (data not herein presented) provided essentially the same results when considering the embankment unsaturated. So, results shown in Figure 8, obtained assuming a saturated dam, can be taken as representative of permanent flow conditions developed at the site in the initially unsaturated, homogeneous earth fill dam.

It has, however, to be noted that a unique laboratory SWRC, obtained from vertically molded specimens under zero confining stresses, was employed to simulate variable conditions of effective stress consolidation and hydraulic anisotropy. As reported by several authors, the SWRC is affected by both such conditions (e.g. Vanapalli et al 1999; Habasimbi & Nishimura 2018; Roy & Rajesh 2018, 2019; Zhou & Chen, 2021; Jadar et al., 2023). However, the shape of the SWRC typically does not change much, particularly at higher degrees of saturation, with the saturated permeability of the soil specimen being mandatory in most cases. An example of that is given by Priono et al. (2017). These authors evaluated effects of hydraulic anisotropy on unsaturated soils and showed that the use of anisotropic ratios defined based on the saturated soil is also applicable to unsaturated soils as herein assumed.

Unsurprisingly, results showed that soil permeability directly affects hydraulic gradient behavior and is likely to increase when permeability decreases. This pattern can be understood using flow nets with squares configuration. Lower permeability coefficients generate a concentration of equipotential lines, perpendicular to two consecutive flow lines, defining a given distance (within two consecutive equipotential lines) in a square of the flow net in which the hydraulic gradient is being accessed. That causes a total head decrease in a smaller distance, increasing gradients (e.g. Norouzi et al., 2020).

Equivalent 2D and 3D seepage analyses considering permeability coefficients from laboratory tests were not able to justify an internal erosion process. Indeed, critical hydraulic gradients were obtained only in view of the 3D scenarios indicated in Table 8.

Table 8. Scenarios resulting in critical gradients - isotropic conditions.

Scenario	*k* (m/s)	*i*	Height of the PLEP (m)
5	4.0×10^{-9}	1.00	3.11
5	4.0×10^{-10}	1.17	3.18
5	4.0×10^{-11}	1.19	3.20
6	4.0×10^{-10}	0.95	1.81
6	4.0×10^{-11}	0.99	1.81

Results related to the height of the PLEP in Scenario 6 (section 1 to 4 m wide along the spot point) can be disregarded as they are not representative of the location of the exit point of the phreatic line defined based on the field instrumentation data. Considering Scenario 5 (region corresponding to one third of the maximum height of the dam from the toe of the downstream slope), it is shown that a material with saturated isotropic permeability lower than $4x10^{-9}$ m/s would be required to lead to critical conditions.

As indicated in Table 3, saturated permeability of samples taken from different depths of the embankment was some 10 to 100 times greater than the one that could promote a critical condition at the site (order of 10^{-9} m/s). On the other hand, at the spot point (Table 4) vertical and longitudinal saturated permeabilities obtained in tests under 50 and 100 kPa of effective stresses are of such order of magnitude. However, further results of 3D analyses considering anisotropy of permeability under $\sigma' = 100$ kPa confirmed that critical hydraulic conditions, under representative height of the PLEP, would only occur in the case of Scenario 5.

Both 2D and 3D seepage numerical analyses indicated that hydraulic gradients tend to increase when water flows through a lower permeability material. Furthermore, considering laboratory data, only in presence of a specific compacted layer with isotropic or anisotropic permeability (Scenario 5), critical hydraulic gradients would occur. It is, however, difficult to accept that such a condition could have been developed at the time the embankment was built. Thus, it is hypothesized that the natural evolution of vegetation throughout the years of operation of Dam X might have had an important role in the observed piping phenomena.

Aubertin (1971) affirms that a soil in which a root has grown and then rotted can sustain pipes with fines being carried under a constant water flux. With that, however, it would be expected to have increased vertical and horizontal saturated permeabilities of the originally compacted material. On the other hand, decomposition of organic matter from vegetation and, particularly, increased soil suction provided by a growing vegetation could imply in the occurrence of lower enough permeabilities at a specific site. Although fortuitous, that could explain the herein-obtained numerical results. No information on these, particularly on the possibility of having anisotropy in the horizontal plane, was found in the current literature.

4. Conclusion

This work was developed in an attempt to find possible causes of fines being carried throughout an old, and with low maintenance dam. The dam history was evaluated. Field and laboratory investigations were performed, and extensive 2D and 3D seepage analyses were developed.

Unsaturated water flow analyses were run considering both field monitoring data, and results of laboratory tests. It was verified that obtained saturated permeability coefficients were not able to provide initiation of an internal erosion process in the point of the Dam where occurrence of such process was identified. Indeed, critical hydraulic gradients were obtained only in 3D analyses considering saturated permeability coefficients below 10^{-9} m/s.

Based on these findings, on the fact that Dam X was covered by vegetation, including large trees, and in agreement with a few literature data, it is proposed here that the occurrence of somehow specific root distribution in a section of the downstream slope may have generated a soil with relatively homogeneous permeability coefficient lower than $1.0x10^{-9}$ m/s, promoting the anomaly observed at Dam X.

Further research is required to support this conclusion, including laboratory experiments such as pinhole tests to better predict critical hydraulic gradient values under unsaturated conditions; effects of organic debris content and its influence on saturated permeability coefficients and investigation of internal erosion resistance in presence of root systems.

Nonetheless, the analyses presented in this study provide valuable insights into the complex interactions between vegetation and internal erosion processes in earth fill dams, highlighting the need for careful monitoring and maintenance, especially in aging structures. Future research on the influence of root systems, organic debris, and permeability variations in dams will be essential for developing more robust guidelines for dam management and erosion prevention. Studies such as these may contribute to a broader understanding of dam safety, not only improving local practices but also field standards generalization.

Acknowledgements

This work was developed within the context of the PRONEX Project E-26/210.920/2016 (208891) supported by FAPERJ (Research Supporting Foundation from the Rio de Janeiro State) and CNPq (Brazilian Council on Scientific and Technological Development). The first author acknowledges CAPES by its post-graduation grant support. The authors are also grateful to ALTA Geotecnia Ambiental for providing basic data used in the development of the research work and to the Environmental and Geotechnical Laboratory of the Pontifical Catholic University of Rio de Janeiro where the laboratory tests were performed.

Declaration of interest

The authors have no conflicts of interest to declare. All co-authors have observed and affirmed the contents of the paper and there is no financial interest to report.

Authors' contributions

Conrado Oliveira Carestiato de Carvalho: conceptualization, data curation, investigation, methodology, laboratory tests, formal analyses, writing – original draft. Tácio Mauro Pereira de Campos: conceptualization, supervision, project administration, validation, funding acquisition, critical review of the manuscript. Álvaro de Freitas Viana: conceptualization, project administration, critical review of the manuscript.

Data availability

The datasets generated and analyzed in the course of the current study are available from the corresponding author upon request.

Declaration of use of generative artificial intelligence

This work was not prepared with the assistance of generative artificial intelligence. The authors assume full responsibility for the content of the publication.

List of symbols and abbreviations

i Hydraulic gradient
i_{cr} Critical hydraulic gradient
k_{sat} Saturated permeability
m_f Fredlund & Xing (1994) Coefficient; material parameter which is primarily a function of the residual water content
n_f Fredlund & Xing (1994) Coefficient; material parameter which is primarily a function of the rate of water extraction from the soil once the air-entry value has been exceeded
PLEP Phreatic line exit point
a_f Fredlund & Xing (1994) Coefficient; material parameter which primally related to the air-entry value of the soil.
σ' Effective stress
Ψ_r Suction at the residual water content

References

ABNT NBR 6457. (2016a). *Soil samples – Preparation for compaction and characterization test*. ABNT - Associação Brasileira de Normas Técnicas, Rio de Janeiro, RJ. (in Portuguese).

ABNT NBR 7180. (2016b). *Soil – Plasticity limit determination*. ABNT - Associação Brasileira de Normas Técnicas, Rio de Janeiro, RJ. (in Portuguese).

ABNT NBR 6458. (2016c). *Gravel grains retained on the 4.8 mm mesh sieve – Determination of the bulk specific gravity of the apparent specific gravity and of water absorption*. ABNT - Associação Brasileira de Normas Técnicas, Rio de Janeiro, RJ. (in Portuguese).

ABNT NBR 6459. (2017). *Soil – Liquid limit determination*. ABNT - Associação Brasileira de Normas Técnicas, Rio de Janeiro, RJ. (in Portuguese).

ABNT NBR 7181. (2018). *Soil – Grain size analysis*. ABNT - Associação Brasileira de Normas Técnicas, Rio de Janeiro, RJ. (in Portuguese).

ASTM D5298. (2016). *Standard Test Method for Measurement of Soil Potential (Suction) Using Filter Paper*. ATMS International, West Conshohocken, PA. https://doi.org/10.1520/D5298-16.

Aubertin, G.M. (1971). *Nature and extent of macropores in forest soils and their influence on subsurface water movement*. Upper Darby, PA: U.S. Department of Agriculture, Forest Service, Northeastern Forest Experiment Station.

Babu, G.L.S., & Vasudevan, A.K. (2008). Seepage velocity and piping resistance of coir fiber mixed soils. *Journal of Irrigation and Drainage Engineering*, *134*(4), 485-492. http://dx.doi.org/10.1061/(ASCE)0733-9437(2008)134:4(485).

Bernatek-Jakiel, A., Vannoppen, W., & Poesen, J. (2017). Assessment of grass root effects on soil piping in sandy soils using the pinhole test. *Geomorphology*, *295*, 563-571. http://dx.doi.org/10.1016/j.geomorph.2017.08.027.

Carvalho, T.M.O., Campos, T.M.P., Hernandez, M.P.M., & Antunes, F.S. (2006). Study of shear strength and physical-mineralogical characteristics of a saprolitic soil percolated by a caustic liquor. In *12º Congresso Brasileiro de Mecânica dos Solos e Engenharia Geotécnica* (pp. 1723-1728). Curitiba, Brazil. (in Portuguese).

De Carvalho, C.O.C. (2022). *Initiation of internal erosion processes in homogeneous earth dam: a case study* [Master's dissertation]. Civil and Environmental Engineering Department, PUC-Rio. (in Portuguese).

De Mello, V.F.B. (1975). Some lessons from unsuspected, real and fictitious problems in earth dam engineering in Brazil. In *6th Regional Conference for Africa on Soil Mechanics & Foundation Engineering* (pp. 285-304). Durban, South Africa.

Delgado-Ramos, F., Poyatos, J.M., & Osorio, F. (2012). Internal erosion of clayey soil protected by granular filters. *Houille Blanche*, 98(4-5), 42-47. http://dx.doi.org/10.1051/lhb/2012029.

Fell, R., Wan, C.F., Cyganiewicz, J., & Foster, M. (2003). Time for development of internal erosion and piping in embankment dams. *Journal of Geotechnical and Geoenvironmental Engineering*, *129*(4), 307-314. http://dx.doi.org/10.1061/(ASCE)1090-0241(2003)129:4(307).

Foster, M.A., & Fell, R.A. (1999). *Framework for estimating the probability of failure of embankment dams by internal erosion and piping using event tree methods*. Retrieved in November 3, 2024, from https://vm.civeng.unsw.edu.au/uniciv/R-377.pdf.

Foster, M.A., Fell, R., & Spannagle, M. (2000). The statistics of embankment dam failures and accidents. *Canadian Geotechnical Journal*, *37*(5), 1000-1024. http://dx.doi.org/10.1139/t00-030.

Fredlund, D.G., & Xing, A. (1994). Equations for the soil-water characteristic curve. *Canadian Geotechnical Journal*, *31*(4), 521-532. http://dx.doi.org/10.1139/t94-061.

Habasimbi, P., & Nishimura, T. (2018). Comparison of soil-water characteristic curves in one-dimensional and isotropic stress conditions. *Soil Systems*, *2*(3), 43. http://dx.doi.org/10.3390/soilsystems2030043.

Head, K.H. (1994). *Manual of Soil Laboratory Testing - Volume 2: Permeability, Shear Strength and Compressibility Tests*. John Wiley & Sons.

Jadar, C.M.; Rajesh S. & Roy, S. (2023). The effect of stress-dependent SWRC in the load carrying capacity of the slope subjected to the drying-wetting path. *E3S Web of Conference*, *382*, 12004. https://doi.org/10.1051/e3sconf/202338212004.

Keaton, J.R. (2018). Dispersivity. In: Bobrowsky, P., Marker, B. (Eds.), *Encyclopedia of Engineering Geology. Encyclopedia of Earth Sciences Series*. Cham: Springer. https://doi.org/10.1007/978-3-319-12127-7_92-1

Kenney, T.C., & Lau, D. (1985). Internal Stability of granular filters. *Canadian Geotechnical Journal*, *22*(2), 215-225. http://dx.doi.org/10.1139/t85-029.

Kezdi, A. (1979). *Soil Physics-Selected Topics.* Elsevier Scientific Publishing.

Li, M., & Fannin, R.J. (2008). Comparison of two criteria for internal stability of granular soil. *Canadian Geotechnical Journal*, *45*(9), 1303-1309. http://dx.doi.org/10.1139/T08-046.

Moncada, M.P.H., Campos, T.M.P., Antunes, F.S., & Bertolino, A.V.F.A. (2005). Evaluation of moisture-suction characteristics of a lateritic soil submitted to infiltration by caustic liqueur. In *International Symposium on Advanced Experimental Unsaturated Soil Mechanics* (pp. 377-383). London, UK.

Mungan, N. (1965). Permeability reduction through changes in pH and salinity. *Journal of Petroleum Technology*, *17*(12), 1449-1453.

Norouzi, R., Salmasi, F., & Arvanaghi, H. (2020). Uplift pressure and hydraulic gradient in Sabalan Dam. *Applied Water Science*, *10*, 111. http://dx.doi.org/10.1007/s13201-020-01195-2.

Oliveira, E.P. (2006). *Bio-physical-chemical-mineralogical and micromorphological characterization of a granite-gneissic weathering profile from Curitiba, PR* [Master's dissertation]. Civil and Environmental Engineering Department, PUC-Rio.

Perry, E.B. (1975). *Piping in earth dams constructed of dispersive clay: literature review and design of laboratory tests*. Retrieved in November 3, 2024, from https://digital.library.unt.edu/ark:/67531/metadc303954/m2/1/high_res_d/metadc303954.pdf.

Priono, P., Rahardjo, H., Chatterjea, K., & Leong, E.C. (2017). Laboratory investigation on hydraulic anisotropy behavior of unsaturated soil. *Canadian Geotechnical Journal*, *54*(7), 1034-1046. http://dx.doi.org/10.1139/cgj-2016-0023.

Roy, S., & Rajesh, S. (2018). Influence of confining pressure on water retention characteristic of compacted soil. *Indian Geotechnical Jr.*, *48*, 327-341. http://dx.doi.org/10.1007/s40098-017-0265-3.

Roy, S., & Rajesh, S. (2019). Simplified model to predict features of soil-water retention curve accounting for stress state conditions. *International Journal of Geomechanics*, *20*(3), http://dx.doi.org/10.1061/(ASCE)GM.1943-5622.0001591.

Sherard, J.L. (1953). *Influence of soil properties and construction methods on the performance of homogeneous earth dams* [Doctoral Thesis]. Harvard University.

Sherard, J.L., Decker, R.S., & Dunnigan, L.P. (1976). Identification and nature of dispersive soils. *Journal of the Geotechnical Engineering Division*, *102*(GT4), 287-301.

Sherard, J.L. (1979). Sinkholes in dams of coarse, broadly graded soils. In *13th International Congress on Large Dams* (pp. 25-35). New Delhi, India.

Suarez, D.L., Rhoades, J.D., Lavado, R., & Grieve, C.M. (1984). Effect on pH on saturated hydraulic conductivity and soil dispersion. *Soil Science Society of American Journal*, *48*(1), 50-55. https://doi.org/10.2136/sssaj1984.03615995004800010009x.

Taher, Z., & Alshibli, K. (2015). *Piping effect in earth dams internal erosion: an investigative paper*. Retrieved in November 3, 2024, from https://www.academia.edu/36203287/PIPING_EFFECT_IN_EARTH_DAMS_An_Investigative_Paper_Prepared_by

Terzaghi, K., Peck, R.B., & Mesri, G. (1996). *Soil Mechanics in Engineering Practice*. Wiley-Interscience.

Turgut, A., Isik, N.S., & Kasapoglu, K.E. (2017). Investigation of factors affecting the dispersibility of clays and estimation of dispersivity. *Bulletin of Engineering Geology and the Environment*, *76*, 1051-1073. http://dx.doi.org/10.1007/s10064-016-0935-x.

Vanapalli, S.K., Fredlund, D.G., & Pufahl, D.E. (1999). The influence of soil structure and stress history on the soil–water characteristics of a compacted till. *Geotechnique*, *49*(2), 143-159.

Vaughan, P., & Soares, H.F. (1982). Design of filters for clay cores of dams. *Journal of the Geotechnical and Geoenvironmental Engineering*, *108*, GT1.

Xu, P., Zhang, Q., Qian, H., Yang, F., & Zheng, L. (2020). Investigating the mechanism of pH effect on saturated permeability of remolded loess. *Engineering Geology*, *284*, http://dx.doi.org/10.1016/j.enggeo.2020.105978.

Zhou, C., & Chen, R. (2021). Modelling the water retention behaviour of anisotropic soils. *Journal of Hydrology (Amsterdam)*, *599*, 126361. http://dx.doi.org/10.1016/j.jhydrol.2021.126361.